THE BELL SYSTEM
TECHNICAL JOURNAL

VOLUME XLIV DECEMBER 1965 NUMBER 10

Measurements of Electromagnetic Backscattering from Known, Rough Surfaces*

By JACQUES RENAU and JAMES A. COLLINSON

(Manuscript received August 20, 1965)

We have measured the cross section for backscattering of laser beams from rough aluminum surfaces and a magnesium oxide slab. These surfaces were specially prepared and their statistical properties were measured. The laser wavelengths were $\lambda = 0.63$, 1.15, and 3.39μ, and both parallel and perpendicular polarizations were used. The angle of incidence was varied from 0° to 89°. In these experiments the ratio of the surface rms height h (from the mean surface) to the wavelength λ is larger than 1/4; for such surfaces the cross section for backscatter at normal incidence is inversely proportional to the square of the rms surface slope, h/l, and is independent of wavelength. At large angles of incidence the cross section increases with increasing slope and also with increasing h/λ, approaching an upper limit which appears to be predicted by a Lambert scattering law. The angular dependence of the cross section differs for the two polarizations; at grazing incidence the cross section is larger for the parallel polarization. The published characteristics of the angular dependence of the cross section of microwave backscattering from the sea and the moon are in remarkable agreement with the backscattering cross section obtained from the various randomly-rough laboratory prepared surfaces at all angles of incidence. Comparison of the laboratory results with published moon data yields for the moon surface an rms height of 40 ± 10 cm, a mean correlation distance or mean scale size of 2.8 ± 0.7 meters,

* A summary of this paper was presented at the URSI Commission 2 April 1965 meeting in Washington, D.C.

an rms slope of 8° ± 4°, and a dielectric constant ε at microwave frequencies of 1.9 ± 0.3 gigacycles.

I. INTRODUCTION

Measurements of backscattering of electromagnetic (EM) waves from rough surfaces have been performed in the past using microwaves scattered from moon, sea and terrain surfaces. Among others, we refer to the experimental work of Davies and Macfarlane,[1] Grant and Yaplee,[2] Wiltse et al[3] and Evans and Pettengill.[4] More recently there has also been interest in backscattering of EM waves from rough overdense plasma surfaces, particularly near grazing angles of incidence.

In order to relate the measurement of backscattering of EM waves from randomly-rough surfaces to the characteristics of the scattering surface, the statistical properties of such surfaces must be independently measured. The bulk of EM wave scatter measurements from randomly-rough surfaces with gentle slopes consists of those obtained from the sea. Although efforts have been made to specify the state of the sea by means of the prevailing winds at the time of the experiment, the statistical parameters of the rough sea surfaces and of the moon have been matters of conjecture based on many untested assumptions. On the other hand, a direct statistical study of the surface irregularities of the moon is impossible, at present, and very difficult for the sea. For these reasons, the use of randomly-rough surfaces specially prepared for a scatter experiment was desirable and furthermore, was necessary to test the range of validity of the available rough-surface scattering theories. Surface preparation for such scatter experiments at microwave frequencies is a formidable task because of the following requirements: the mean height correlation distance (or scale size) l of the surface should be much larger than the wave length λ to correspond to most cases of physical interest, the beam diameter d must be much larger than l in order to make the scattering area a representative member of the statistical ensemble, and the largest dimension L of the scattering surface must be much larger than d so that all of the beam is intercepted even near grazing incidence. Thus in order to perform a meaningful experiment one requires that $L \gg d \gg l \gg \lambda$. At optical frequencies, however, where $\lambda \cong 1$ micron, the above requirements are satisfied when $l =$ tens of microns, $d =$ few mm, and $L =$ tens of cm, and the scaled down experiment can be performed conveniently in the laboratory with compact prepared surfaces. Lasers provide the beam power, directionality, spatial coherence and monochromaticity needed for successful measurements of backscattering at optical frequencies. Moreover, a He-Ne gas laser can be operated at a wavelength of 0.6328 (hereafter referred to as 0.63) 1.15, or 3.39 microns

simply by changing the cavity mirrors, so that wavelength dependence of backscattering is easily measured.

Reported in this paper are the results obtained from a laser backscatter experiment using prepared and statistically studied randomly-rough metallic surfaces at angles of incidence varying continuously from 0° (normal) to 89°, for parallel and perpendicular polarizations and for differing wavelengths. (Parallel and perpendicular polarization refer to the orientation of the electric field with respect to the plane of incidence. Workers describing the sea data use a different nomenclature. Our parallel polarization is equivalent to their vertical polarization and our perpendicular polarization is equivalent to their horizontal polarization.) We will describe first the preparation of the surfaces and the measurement of their statistical properties. The latter are the relevant correlation functions, height distributions, the rms height, and the mean height correlation distance. We will then give the arrangement for the backscatter measurements and the experimental results.

II. PREPARATION OF THE SURFACES AND THEIR STATISTICAL PROPERTIES

Ten by 22 cm flat aluminum surfaces were blasted at various pressures with hard alumina grits. One of the surfaces was blasted with sizes distributed from very small up to approximately 200 microns, another with sizes distributed up to approximately 100 microns, and a third surface was blasted with steel spheres of sizes distributed from very small up to 44 microns. In order to remove sharp edges caused by the blasting, we experimented with various methods of polishing, such as chemical polishing, electroplating, and electropolishing. Electropolishing was used since this process removed material more from the protrusions than from the valleys. Fig. 1 is a perspective view of one surface. The 3-inch ruler next to the surface in Fig. 1 is used for comparison of dimensions. In Fig. 2 we show the microscopic views at normal incidence of all three rough surfaces.

Contour traces or profiles of the surface irregularities were obtained at various locations both within and without the area illuminated by the laser beam, after the backscatter measurements were completed in order to avoid any possible damage to the surfaces. For each location, the tracing was done over a length of 2 cm, a distance which was found to be much larger than the mean correlation length of any of the surfaces.

The traces were obtained with a stylus which ran along the surface in a manner analogous to a phonograph pickup. The stylus pressure was kept low enough so that there was no detectable distortion of the surface. The radius of the stylus of 13 micron was measured by a Bausch and Lomb optical comparitor. A short sample of these traces for each of the

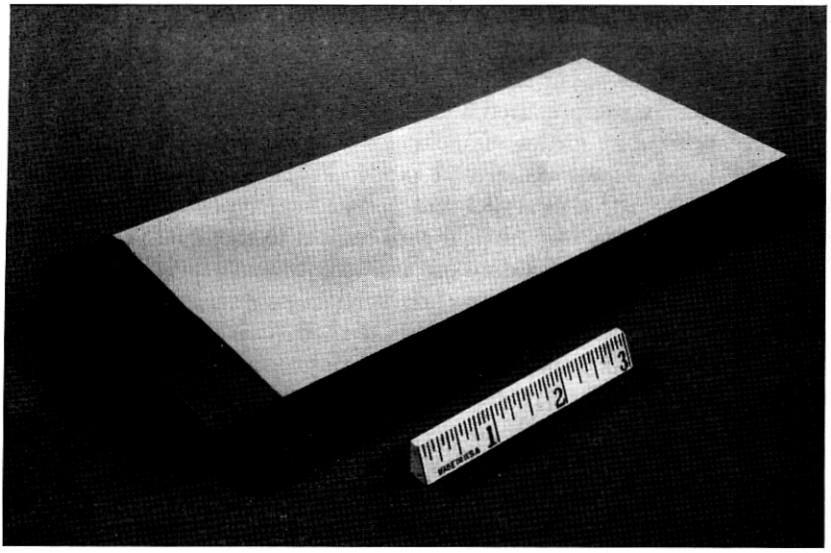

Fig. 1 — View of one of the aluminum surfaces.

aluminum surfaces is shown in Fig. 3. The estimated effective radius of the stylus at a depth of 1 micron in the surface is approximately 5 microns; at a depth of 2 microns it is 7.5 microns and at a depth of 13 microns or more the radius of the stylus should approach the constant

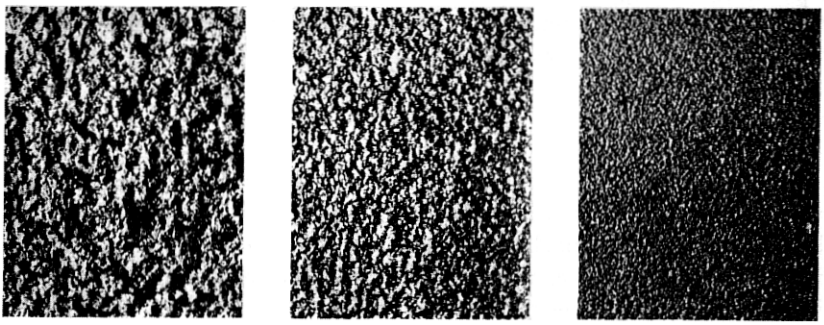

(a) SURFACE NO. 1
BLASTED WITH NO. 60 QUARTZ GRIT AND ELECTROPOLISHED
MAGNIFICATION 42X

(b) SURFACE NO. 2
BLASTED WITH 150 MESH Al_2O_3 AND ELECTRO-POLISHED
MAGNIFICATION 42X

(c) SURFACE NO. 3
BLASTED WITH STAINLESS STEEL BALLS AND ELECTROPOLISHED
MAGNIFICATION 42X

Fig. 2 — Microscopic views of the rough surfaces.

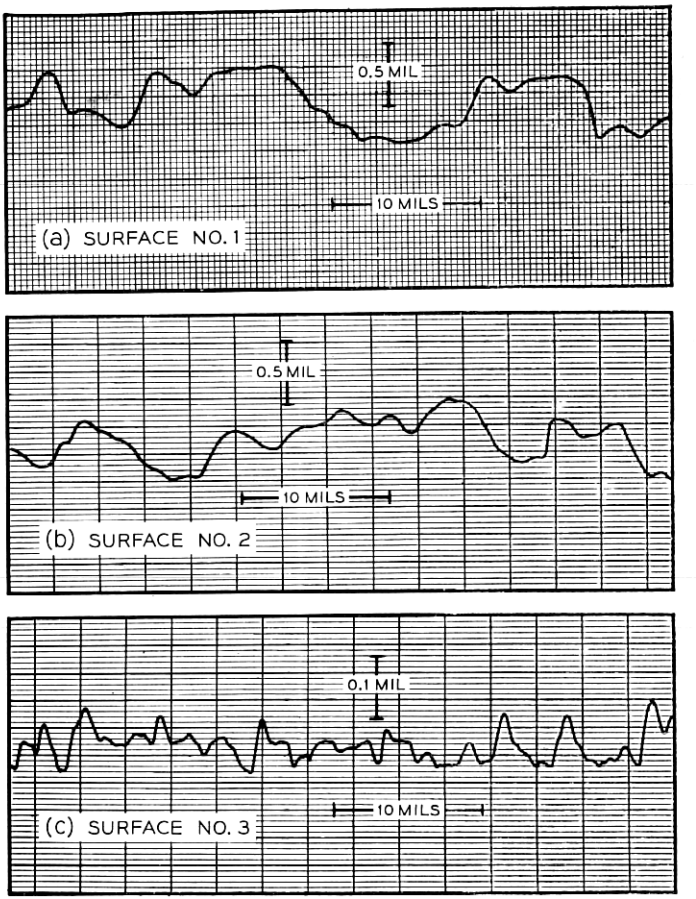

Fig. 3 — Portions of the profile traces of the rough surfaces.

value of 13 microns. Since the mean height correlation distance (mean scale size) obtained for each of the surfaces was much larger than the effective stylus radius, we believe the measured values truly represent the mean correlation distances l. Photo-micrographs of the cross section of the surface irregularities shown in Fig. 4 do not indicate any unusual irregularities which the stylus would be incapable of measuring.

These contour traces were used to obtain the normalized autocorrelation functions of the surfact heights for each of the surfaces. The height autocorrelation function $\tau(\xi)$ was obtained from the contour traces of the surface heights $Z(\rho)$ by calculating for each 2-cm long trace

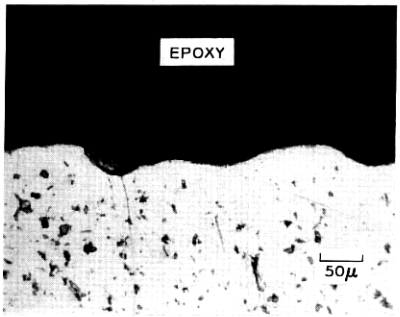

(a) SURFACE NO. 1 (200X APPROX.)

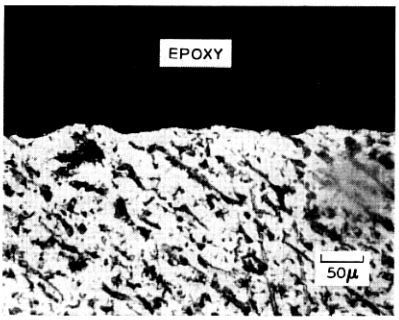

(b) SURFACE NO. 2 (200X APPROX.)

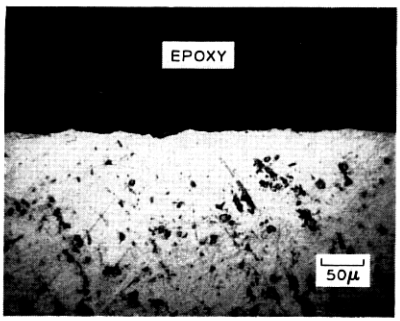

(c) SURFACE NO. 3 (200X APPROX.)

Fig. 4 — Photo-micrographs of the cross section of the rough surfaces.

$$\tau(\xi) = \frac{\frac{1}{3200}\sum_{i=1}^{3200} Z(\rho_i)Z(\rho_i + \xi)}{\frac{1}{3200}\sum_{i=1}^{3200} Z(\rho_i)Z(\rho_i)}$$

where $\rho_i = (x_i^2 + y_i^2)^{\frac{1}{2}}$ represents the position of ith element of height on the average surface and the separation distance ξ was successively increased in integral multiples of 4 microns. Since several 2-cm profiles were obtained at various parts of each surface, a collection of normalized autocorrelation functions for that surface resulted, and these are shown superimposed in Fig. 5 for surfaces No. 1, 2, and 3.

It may be remarked that the analytical function

$$\tau(\xi) = \sin\left[\frac{\pi}{2}\exp\left(-\frac{2}{\pi}\frac{|\xi|}{l}\right)\right],$$

used to fit the experimental correlation data of turbulent media by Corrsin and Kistler[5] and to the studies of wakes from bodies in high

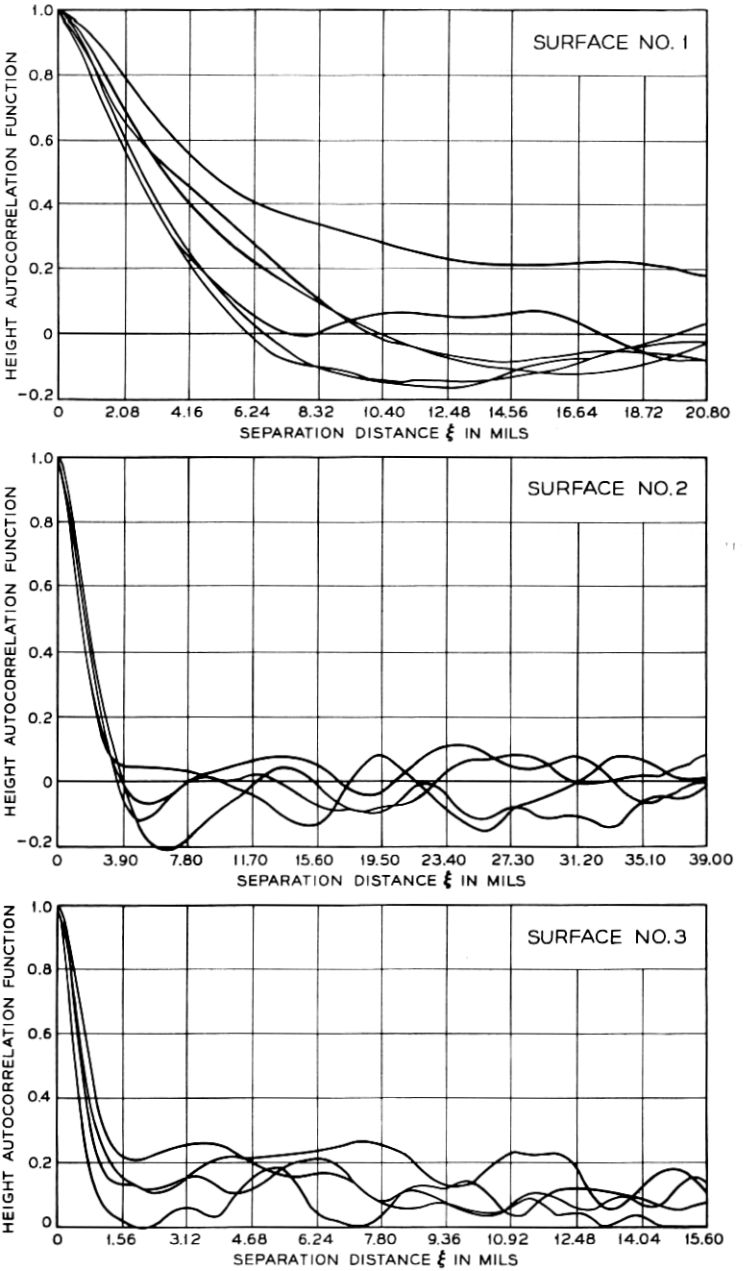

Fig. 5 — Normalized height autocorrelation function (with zero mean) of rough surfaces No. 1, 2, and 3. (Multiple curves represent sampling of various locations of each surface).

speed flight by Schapker,[6] also fits the experimentally obtained autocorrelation functions in our Fig. 5 over a wide range of separation distances ξ. However,

$$\tau(\xi) = \exp\left[-\frac{\left(\frac{\xi}{l}\right)^2}{2\left(1+\frac{|\xi|}{2l}\right)}\right]$$

has equivalent properties as the sine function, and fits the data almost as well, with a very slight change of mean scale size.

The experimental normalized autocorrelation functions, at their half value, have been used to estimate the mean height correlation distance l of the surfaces. The rms height from the zero mean height for each of the surfaces was, by definition, the square root of the unnormalized autocorrelation function at $\xi = 0$. The results of the studies for each of the aluminum surfaces as well as an additional surface (MgO Slab) that will be discussed later are given in Table I. We estimate a standard deviation of the order of $\frac{1}{4}$ of the values of h and l shown above. Since the results of Table I are independent of direction taken on the surface, we conclude the surface irregularities are statistically isotropic.

Also from the traces, the height distributions obtained at least at five different locations for each surface were averaged and are shown in histogram form in Fig. 6 for surfaces 1, 2, and 3. Because of the average shape of the height distribution it seems one may conclude that the statistical characteristics of the surface irregularities although not strictly Gaussian, may be approximated by a Gaussian distribution. We now describe the scatter experiments performed with these surfaces.

III. EXPERIMENTAL ARRANGEMENT

The arrangement of the experiment is shown in Fig. 7. The He-Ne laser tube had an overall length of 120 cm, a discharge length of 100 cm, and a tube bore of 5 mm. By using the proper mirrors, the laser was made to oscillate at 0.63μ, 1.15μ, or 3.39μ. The laser beam was plane polarized with an orientation determined by the Brewster-angle windows of the

TABLE I

	Al Surfaces			MgO Slab
Surface number	1	2	3	
rms height h from the mean height	7μ	3μ	1μ	25μ
Mean correlation distance l	50μ	26μ	10μ	90μ
rms slope h/l	1/7.1	1/8.6	1/10	1/3.6

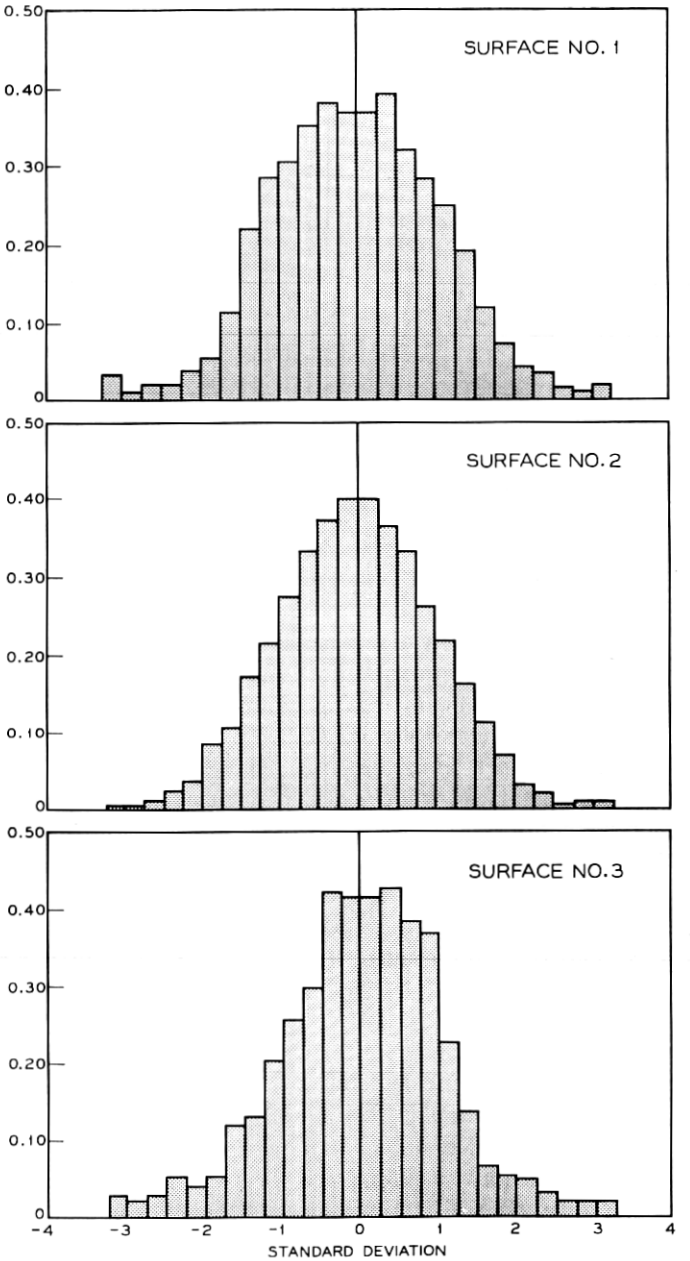

Fig. 6 — Average distribution of surface heights for surfaces No. 1, 2, and 3. (Overlapping histograms representing samples at various portions of each surface were used in averaging.)

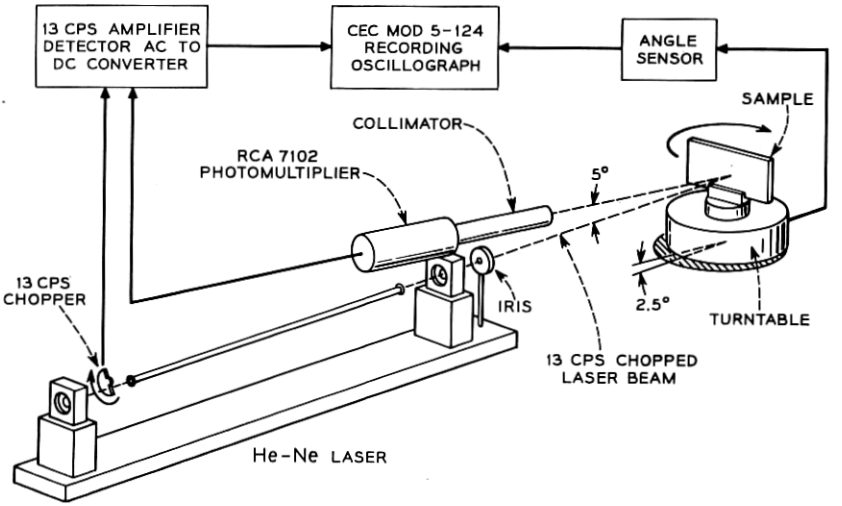

Fig. 7 — Diagram of experimental arrangement.

discharge tube. The diameter of the laser beam was about 4 mm, and it passed through an iris of approximately 4-mm diameter. The beam power was about 10 mw. The beam was incident upon one of the surfaces mounted upon an electronically controlled turntable which carried a protractor. The distance from the front laser mirror to the scattering surface was one meter. At wavelengths of 0.63μ and 1.15μ the relative backscattered energy was measured at all angles of incidence using RCA 7265 and 7102 photomultiplier tubes. The absolute level of backscattering at normal incidence was measured at all three wavelengths by focusing the backscattered energy onto a calibrated thermopile with a quartz lens. The thermopile output power was read with a Keithley Model 149 microvoltmeter.

The turntable was tilted by 2.5° so as to reflect specularly into the center of the detector. The constant speed turntable rotated the sample surface in the path of the incident beam, thus varying continuously the angle of incidence. The angular position of the turntable was calibrated and electronically recorded on an oscillograph. In order to minimize the noise level, the beam was chopped at a rate of 13 cps. The detected signal was amplified by a 13-cps amplifier ac-dc converter and fed simultaneously with the angle information into the oscillograph. The walls of the dark room where the experiment was performed, as well as all protruding objects, were covered with highly absorbent black material. At grazing incidence and with the most weakly backscattering surface, the signal was approximately 10 db above the background noise for both

0.63μ and 1.15μ wavelengths. The power input-output linearity of the over-all system at $\lambda = 0.63\mu$ and 1.15μ were checked by the use of calibrated Kodak neutral filters.

In Fig. 8, we show a retrace of the raw data for one run as observed on the oscillograph. The largest observed fluctuations were much smaller than the width of the line of the redrawn curves. When the gain of the amplifier was increased to give suitable response for the weaker signal at larger angles of incidence the amplified signals did not saturate the equipment over the range of angles for which the data are shown.

IV. RELATION BETWEEN THE MEASURED BACKSCATTERED POWER AND THE BACKSCATTERING CROSS SECTION

It will be helpful in interpreting the data that follow to show the relationship between the backscattered power $P_B(\psi,f)$ incident upon the photomultiplier tube and the radar backscattering cross section $\sigma_B(\psi,f)$

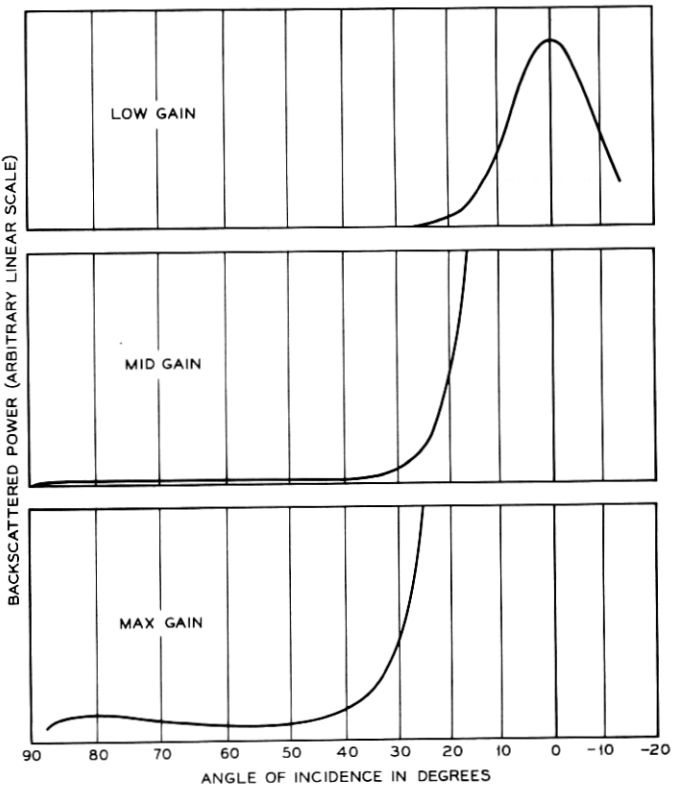

Fig. 8 — Trace of oscillograph raw data.

where f is the frequency of the incident beam, and ψ is the angle of incidence of the beam at the surface. The subscript B denotes the case of backscattering. By definition

$$P_B(\psi,f) = \frac{1}{2\eta} \langle \mathbf{E}_{SB}(\psi,f,R) \cdot \mathbf{E}_{SB}^*(\psi,f,R) \rangle A_{\text{rec}}$$

where $\langle\ \rangle$ denotes the ensemble average of the stochastic backscattered electric field $\mathbf{E}_{SB}(R)$ observed at the receiver located at a distance R from the scattering surface, η is the characteristic impedance of free space and $A_{\text{rec.}}$ is the energy sensitive area of the photomultiplier tube. Let the power incident upon the target at frequency f be denoted by $P_i(f)$, then

$$P_i(f) = \frac{1}{2\eta} |\mathbf{E}_i|^2 A_0,$$

where $|\mathbf{E}_i|$ is the amplitude of the incident electric field, and A_0 is the area of the collimated incident beam and is equal to the area illuminated on the surface at normal incidence. Therefore,

$$\frac{P_B(\psi,f)}{P_i(f)} = \frac{\langle \mathbf{E}_{SB}(\psi,f,R)\mathbf{E}_{SB}(\psi,f,R) \rangle A_{\text{rec}}}{|\mathbf{E}_i|^2 A_0}. \tag{1}$$

Let the numerator and the denominator be multiplied by $4\pi R^2$. For R much larger than any other dimension of interest in the experiment the radar cross section is defined as

$$\sigma(\psi,f) = \frac{4\pi R^2 \langle \mathbf{E}_S(\psi,f,R)\mathbf{E}_S^*(\psi,f,R) \rangle}{|\mathbf{E}_i|^2}$$

and in particular for the case of backscattering

$$\sigma_B(\psi,f) = \frac{4\pi R^2 \langle \mathbf{E}_{SB}(\psi,f,R)\mathbf{E}_{SB}^*(\psi,f,R) \rangle}{|\mathbf{E}_i|^2}. \tag{2}$$

Using (2), (1) may be rewritten as follows:

$$\frac{P_B(\psi,f)}{P_i(f)} = \frac{\sigma_B(\psi,f)}{A_0} \frac{\Omega}{4\pi} \tag{3}$$

where Ω, the solid angle, is defined as

$$\Omega \equiv \frac{A_{\text{rec.}}}{R^2}.$$

We shall therefore use interchangeably the words normalized backscat-

tered power and normalized cross section, since

$$\frac{\dfrac{P_B(\psi,f)}{P_i(f)}}{\dfrac{P_B(0,f)}{P_i(f)}} = \frac{P_B(\psi,f)}{P_B(0,f)} = \frac{\dfrac{\sigma_B(\psi,f)}{A_0}}{\dfrac{\sigma_B(0,f)}{A_0}} = \frac{\sigma_B(\psi,f)}{\sigma_B(0,f)}. \tag{4}$$

In the following pages we shall neglect to use the subscript B since all our results are only for the case of backscattering. For convenience in notation we shall also denote the cross section $\sigma(\psi,f)$ by $\sigma(\psi)$.

V. BACKSCATTERING RESULTS

We will examine first the behavior of the absolute backscattering cross section per unit area at normal incidence $\sigma(0)/A_0$ from each of the surfaces. At normal incidence the data were taken with a photomultiplier ($\lambda = 0.63, 1.15\mu$) as well as with a thermopile detector ($\lambda = 0.63, 1.15$, and 3.39μ) as described earlier. We then will give the cross section measured with a photomultiplier detector for continuously varying angles of incidence. In Figs. 9 to 15, the symbols $E_{||}$ and $E_{\perp}$ refer, respectively, to the parallel and perpendicular orientation of the electric field to the plane of incidence.

5.1 *Absolute Cross Section at Normal Incidence*

Table II displays $P_B(0,f)/P_i(f)$, the ratio of backscattered power to incident power at normal incidence. Referring to (3), the values shown in Table II are also the backscattering radar cross section per unit area at normal incidence times 10^{-4} ($R \approx 100$ cm, $A_{\text{rec.}} \approx 13$ cm^2 or $\Omega/4\pi \approx 10^{-4}$). No measurable difference was found in the results when using 0.63μ or 1.15μ. To obtain the radar backscatter cross section per unit area at normal incidence, $\sigma(0)/A_0$, one adds 40 db to the above values. Had we backscattered from a smooth flat metallic surface, the backscattering cross section per unit area, at normal incidence, would then be calculated on the basis of $[\sigma(0)/A_0]_{\text{smooth}} = 4\pi A_0/\lambda^2$ which for a beam of 2-mm radius and $\lambda \approx 1\mu$ is equal to 82 db. It is interesting to compare this result with those obtained from the rough surfaces at normal incidence.

It is evident that, within experimental error, the cross section, at normal incidence, is independent of wavelength, and that it increases as the rms slope of the surface irregularities decreases. A more quantitative conclusion is given in the section on Discussions and Conclusions. Meas-

TABLE II — RATIO OF BACKSCATTERED POWER TO INCIDENT POWER $P_B(0, f)/P_i(f)$ in DB

	$\lambda = 0.63\mu$ $\lambda = 1.15\mu$	$\lambda = 3.39\mu$
Surface No. 1 (roughest)	-25.5 ± 0.5	-25.0 ± 0.5
Surface No. 2	-24.0 ± 0.5	-23.5 ± 0.5
Surface No. 3 (smoothest)	-23.0 ± 0.5	-22.5 ± 0.5
MgO slab	-32.0 ± 0.5	-32.0 ± 0.5

urements were made with both polarizations, and at normal incidence no dependence on polarization was found implying statistical isotropy of the surface irregularities.

5.2 *Normalized Cross Section vs Angle of Incidence*

The angular dependence of backscattering cross section is most conveniently studied if the data are normalized to unity at normal incidence. This was done for all measurements of backscattering made with continuously changing angle of incidence. These data include dependence on polarization, wavelength, and surface characteristics. In all of the measurements of the angular dependence of cross section, the error did not exceed ± 0.5 db.

The results of the normalized backscattering cross section $\sigma(\psi)/\sigma(0)$

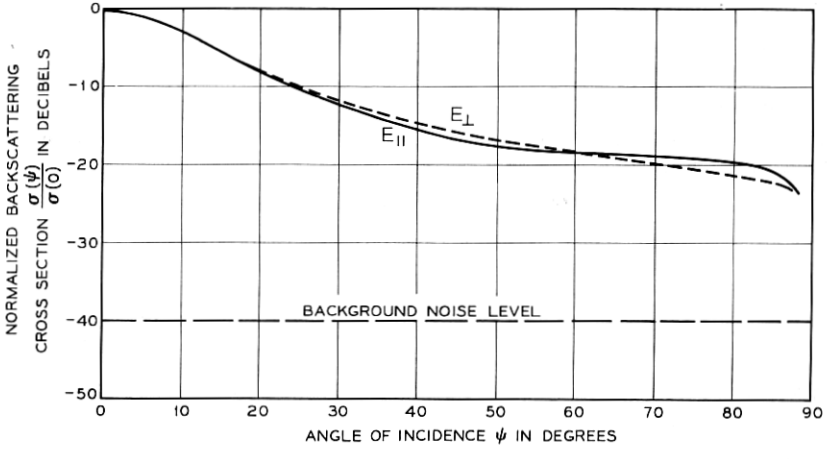

Fig. 9 — Normalized backscattered power of laser beam versus angle of incidence, for both polarization, from rough Al surface No. 1, $h \approx 7\mu$, $l \approx 50\mu$, $\lambda \approx 0.63\mu$.

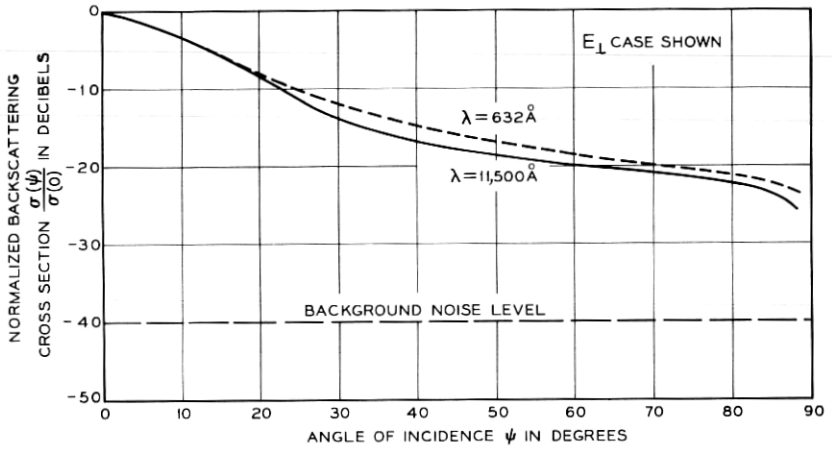

Fig. 10 — Normalized backscattered power of laser beam versus angle of incidence for perpendicular polarization from rough surface No. 1 for wavelengths $\lambda \approx 0.63\mu$ and 1.15μ.

versus angle of incidence ψ for surface No. 1 (roughest aluminum surface) is shown in Fig. 9. The laser wavelength λ was 0.63μ and the results for both the parallel and perpendicular polarizations are included.

Fig. 10 presents a comparison of the results for two wavelengths, 0.63μ and 1.15μ. The perpendicular polarization was used in both cases. We notice that the cross section decreases as the wavelength increases.

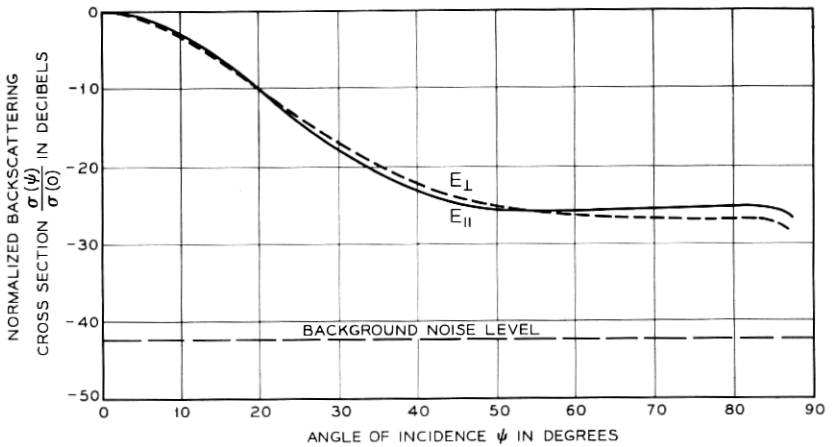

Fig. 11 — Normalized backscattered power of laser beam versus angle of incidence, for both polarization, from rough surface No. 2; $h \approx 3\mu$, $l \approx 26$, $\lambda \approx 0.63\mu$.

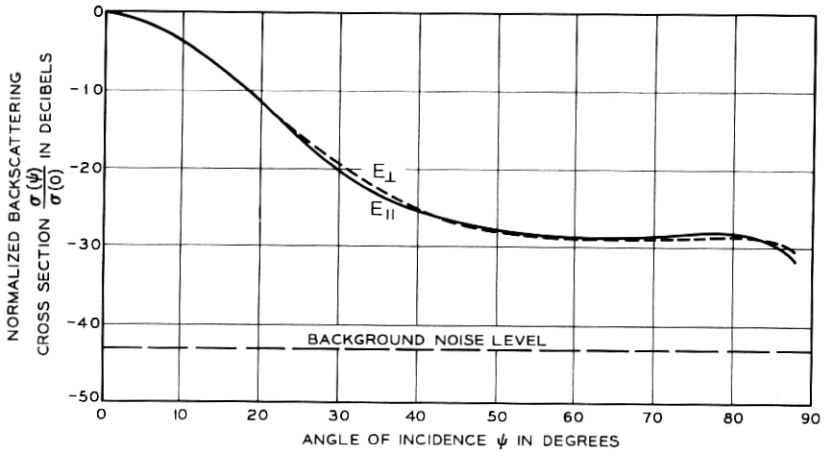

Fig. 12 — Normalized backscattered power of laser beam versus angle of incidence, for both polarization, from rough surface No. 3; $h \approx 1\mu$, $l \approx 10\mu$, $\lambda \approx 0.63\mu$.

The $\sigma(\psi)/\sigma(0)$ versus ψ for surface No. 2 is shown in Fig. 11, which includes curves obtained for both polarizations. The wavelength was 0.63μ.

The normalized cross section $\sigma(\psi)/\sigma(0)$ versus the angle of incidence ψ for surface No. 3 (the least rough of the Al surfaces) is shown in

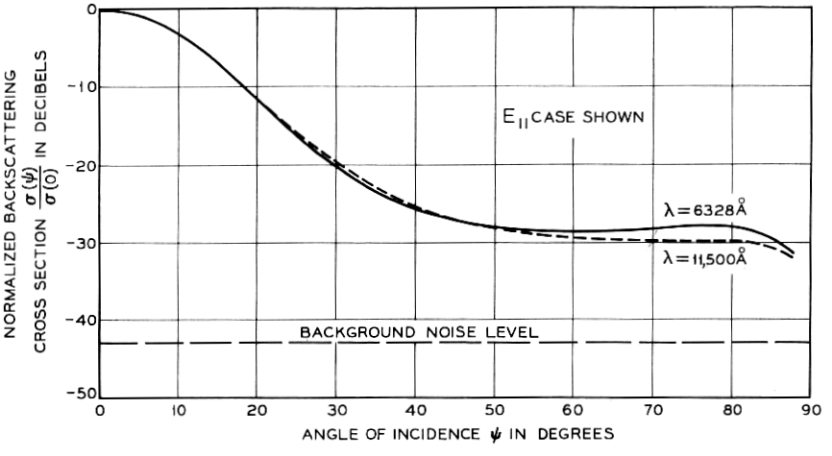

Fig. 13 — Normalized backscattered power of laser beam versus angle of incidence, for both polarization, from rough surface No. 3; $h \approx 1\mu$, $l \approx 10\mu$ and for wavelengths $\lambda \approx 0.63\mu$ and 1.15μ.

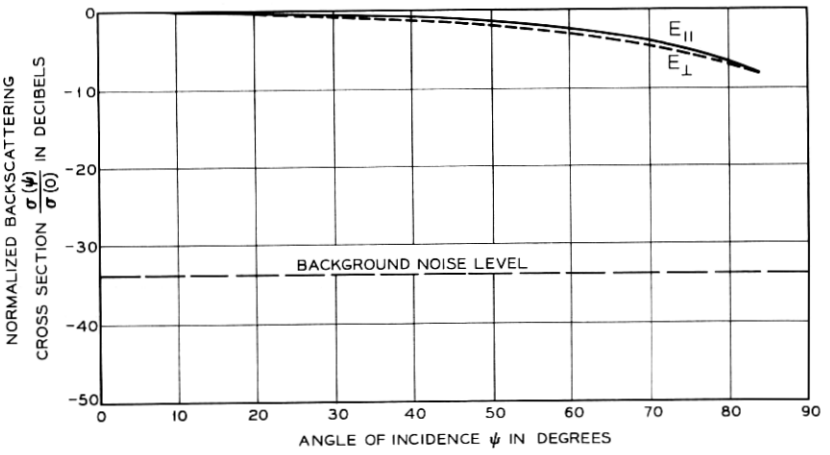

Fig. 14 — Normalized backscattered power of laser beam versus angle of incidence, for both polarization, from the MgO oxide surface; $h \approx 25\mu$, $l \approx 90\mu$, $\lambda \approx 0.63\mu$.

Fig. 12 where the variations with change of polarization are included. The wavelength was 0.63μ. The differences due to the change in polarization seem to be within experimental error, but repeated measurements consistently gave similar differences. The comparison of results at two wavelengths, 0.63μ and 1.15μ, is made in Fig. 13. Again the cross section decreases as the wavelength increases.

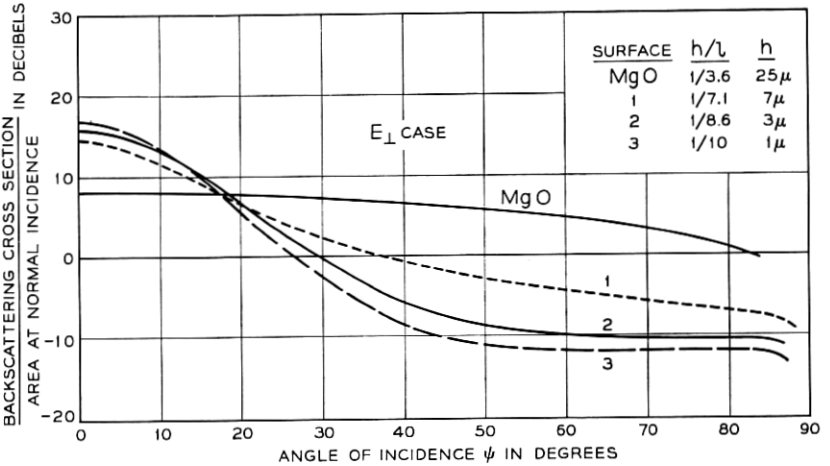

Fig. 15 — Absolute backscattering cross section versus angle of incidence, for the perpendicular polarization from the four rough surfaces; $\lambda \approx 0.63\mu$.

5.3 *Magnesium Oxide as a Very Rough Scattering Surface*

For purposes of comparison, measurements were made of the normalized cross section versus angle of incidence using a slab of magnesium oxide. Microscopic inspection of the MgO powder showed that 90 per cent of the grains of the magnesium oxide were in the range of 20 and 30μ. We thus estimate an rms height of about 25μ for the slab. The mean height correlation size l is estimated to be about 90μ. The normalized backscattering cross section versus ψ is shown in Fig. 14 for both polarizations. The wavelength was 0.63μ. This surface, which has a very large ratio of h/λ and $h/l \approx 1/3.6$, is a cosine law scatterer from 0° to approximately 80°. Therefore, the returned echoes are almost constant over a large range of angles of incidence.

5.4 *Comparison of Data*

The data of all the surfaces were replotted in Fig. 15 to compare surfaces 1, 2, and 3, and that of the MgO slab using the perpendicular polarization and a wavelength of 0.63μ. We note that since the total reflection coefficient of MgO, similar to Al, is near unity at $\lambda = 0.63$ (K. W. Wecht et al, Bell Laboratories Tech. report MM-63-1153-11 August 19, 1963), comparison of the scattering properties of all the surfaces of Fig. 15 is appropriate.

We see that at large angles of incidence (about 50 to 80°) the back cross section increases not only with increasing slope but also with increasing rms height, approaching an angular distribution which is proportional to the cosine of the angle of incidence hereafter loosely referred to as a Lambert scattering law. Moreover as seen from Fig. 15, at grazing incidence a Lambert law scatterer appears to yield the upper limit for the backscattering cross section from rough surfaces. Fig. 15 leads us to conclude also that at normal incidence, such a surface has the least scattering cross section compared to that obtained from any other rough flat surface.

VI. CONCLUSIONS

A careful analysis of the various results of our experiments suggests that the following conclusions may be drawn:

(*i*) Results for the rough metallic surfaces display some common features. The cross section decreases with a negative curvature as the angle of incidence increases, then changes curvature and decreases very gradually for a large range of angles, and finally at grazing angles decreases once more. The last effect is at least partly due to shadowing

produced by the irregularities so that the area illuminated at grazing angles is reduced. If this interpretation is correct, then the experiments indicate that the shadowing effect is not as drastic as thought by some investigators on the basis of qualitative arguments.

Since the above characteristics of backscattering were observed from rough surfaces for which $h/\lambda \gtrsim \frac{1}{4}$ (including the observations at $\lambda = 3.39\mu$ at normal incidence) and at angles of incidence up to 89°, then, using m as a measure of roughness, a surface with irregularities may be considered rough whenever

$$m \equiv \frac{4\pi h}{\lambda} \cos \lambda \gtrsim \frac{1}{10}.$$

Further experiments may show that the lower limit on m can be somewhat smaller than $\frac{1}{10}$, but we feel it will not be very much smaller.

(*ii*) The backscattering radar cross section per unit area at normal incidence from statistically isotropic rough surfaces with $m \gtrsim \frac{1}{10}$ is independent of wavelength and of polarization. The latter is expected because of the statistically isotropic surfaces. The 10 per cent discrepancy observed in comparing $\lambda = 0.63\mu$ and $\lambda = 3.39\mu$ is perhaps due to the fact that at $\lambda = 0.63\mu$ the target is in the near field whereas at $\lambda = 3.39\mu$ the target is almost in the far field (the coherent laser aperture is taken as 2 mm).

(*iii*) The backscattering radar cross section per unit area *at normal incidence* is dependent on the rms slope of the surface and is relatively independent of the rms height. Empirically the slope dependence is well approximated as $\sigma(0)/A_0 = K/(\text{Slope})^2$, where the value of K is approximately $\frac{1}{2}$.

(*iv*) At large angles of incidence (from about 50 to 80°) no simple power law relationship between $\sigma(\psi)/A_0$ and h/l fits the data of Fig. 15. However, $\sigma(\psi)/A_0$ appears to increase (Figs. 10, 13, and 15) with increasing slope h/l, as well as with the rms height h.

(*v*) For $m \gg \frac{1}{10}$ and slope of 1/3.6, the normalized backscatter cross section $\sigma(\psi)/\sigma(0)$ varies as the cosine of the angle of incidence from 0° to nearly 80°. For rough surfaces with larger slope h/l, one would expect that the cosine dependence (Lambert's law) would extend to 90°. In this case, conservation of energy requires that $\sigma(0)/A_0 = 4$. Consequently, when

$$\frac{1}{2} \frac{1}{(\text{slope})^2} \leqq 4$$

the empirical law given in (*iii*) above should be replaced by the constant value of $\sigma(0)/A_0 = 4$. Thus,

$$\sigma(\psi) = 4A_0 \cos \psi \qquad \text{when} \begin{cases} m \gg \frac{1}{10} \\ \frac{h}{l} \gtrsim \frac{1}{2} \end{cases}$$
$$= 4A \cos^2 \psi$$

where $A = A_0 \sec \psi$ is the surface area illuminated.

(*vi*) At large angles of incidence, the backscattering cross section decreases as the wavelength increases. If we assume that the cross section is proportional to $\lambda^{-\gamma}$, then the experiments show that γ is less than 1.20. Our current experiments are directed at determining this wavelength dependence more precisely by the use of wavelengths whose ratio is much larger than the present value of $\lambda_1/\lambda_2 \approx 1.8$.

(*vii*) The difference in backscattering radar cross sections for the two polarizations increases as the angle of incidence is increased. At grazing incidence the cross section is larger for the parallel polarization.

(*viii*) At present we find no theoretical derivation which would account for the observed cross sections and the wavelength dependence over the entire range of angles of incidence.*

VII. COMPARISON WITH SEA AND MOON DATA

The angular dependence of backscattering discussed in (*i*) of the Conclusions is in good agreement with published *sea* and *moon* backscattering measurements for all angles of incidence. This agreement indicates that rough sea surfaces and the moon surface are truly randomly-rough at microwave frequencies. The sea backscattering data of Davies and Macfarlane[1] and Katz,[7] obtained with different conditions of the sea surface, are plotted in Fig. 16 for comparison with our results. Workers reporting sea data customarily normalize the radar cross section of the sea $\sigma(\psi)$ by the area illuminated, A. This area is equivalent to our $A_0 \sec \psi$ in the range of angles where shadowing effects are negligible. Therefore, when comparing the results of our experiments with those for the sea, we note that our $\sigma(\psi)/A_0$ times $\cos \psi$ is their $\sigma(\psi)/A$ (denoted by σ° in their papers). Thus, when comparing quantitatively our $\{\sigma(\psi)/\sigma(0)\}$ with $\{\sigma^\circ(\psi)/\sigma^\circ(0)\}$ for the sea, one should add 10 $\log_{10}$ $\cos \psi$ to our $\sigma(\psi)/\sigma(0)$ expressed in db. The latter quantity may be obtained directly from Fig. 14 since the MgO surface is a cosine law scatterer up to approximately 80°.

Moon reflection data were reported by Evans and Pettengill[4] for 3.6-cm and 68-cm wavelengths. They gave power backscattered as a function

* Although a recent theoretical study[8] finds an expression which reasonably predicts the angular dependence of the cross section, the wavelength dependence at normal incidence is at marked variance with our experimental results (see next section).

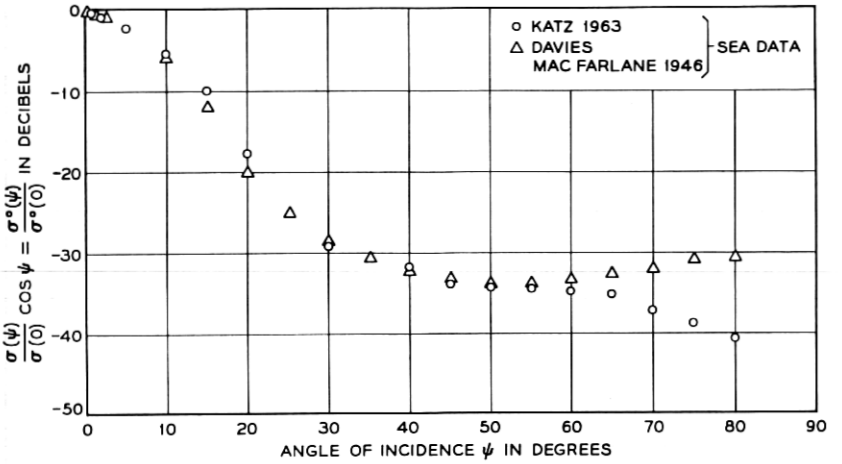

Fig. 16 — Characteristics of sea backscattering data for two differing sea surface conditions.

of delay time τ. We have redrawn their curves giving angle of incidence as the abscissa in our Fig. 17 to allow direct comparison with our results. Their equation (8) has been used which relates delay time for the backscattered power to angle of incidence ψ, i.e., $\cos\psi = 1 - (\tau/11.6)$ where τ is in milliseconds. The moon backscattering data at $\lambda = 0.86$ cm by Lynn et al[9] has also been plotted. Superimposed on the moon data is the

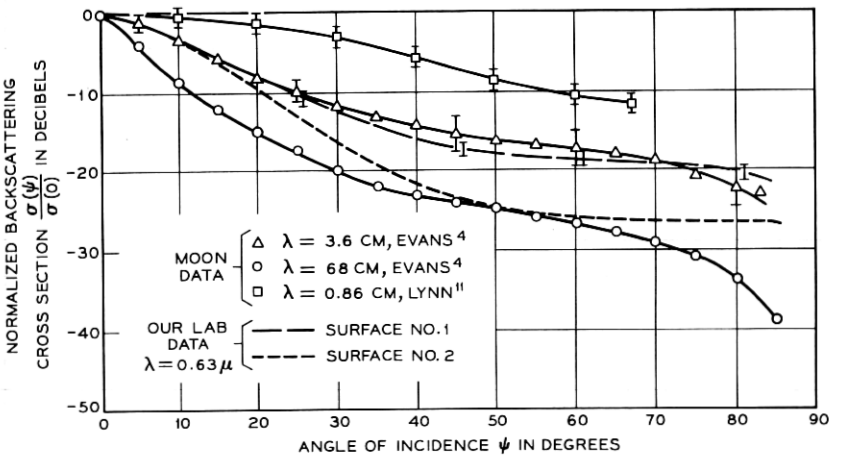

Fig. 17 — Comparison of moon and laboratory backscattering data. (Errors in our laboratory data ±0.5 db all angles. Errors[10] in moon data ±1 db for $\psi \lesssim 30$, ±2 db for $\psi \gtrsim 30$.)

laboratory result obtained from surface No. 1 ($h/\lambda \approx 7/0.63 \approx 11$ and $h/l \approx 1/7.1$) with $\lambda = 0.63\mu$. The curve drawn is the average of both polarizations (shown previously in Fig. 9), since the moon result is an average of both polarizations. Our result from surface No. 2 ($h/\lambda \approx 4.76$ and $h/l \approx 1/8.6$) is also shown. It can be seen that the moon measurements at $\lambda = 3.6$ cm correspond closely to those which one would expect from a randomly-rough surface with parameters similar to our surface No. 1. We have assumed that the variation in the reflection coefficient of the moon with angle of incidence is less than the errors involved in the moon backscattering measurements. This correspondence permits us to estimate the values of the statistical parameters of the moon surface. Thus $h/3.6$ cm ≈ 11 and $h/l \approx 1/7.1$, and hence the parameters of the moon are: rms height $h = 40 \pm 10$ cm (with respect to the mean surface), the mean scale size $l = 2.8 \pm 0.7$ meters, and the rms slope angle is $8° \pm 4°$. Any larger variation in these parameters would cause the laboratory scatter data to fall outside the limits of the error bars of the moon data. These results lead us to conclude that the number of small irregularities on the moon's surface is far greater than the number of big irregularities, such as the lunar mountains.

Using the value for the radar backscattering cross section per unit area for the moon published by Safran,[11] it is possible to calculate an approximate value for the dielectric constant, ε, of the moon at microwave frequencies. The radar cross section per unit area, measured at normal incidence from a metallic surface, at the laboratory, can be compared with that of the moon's surface. The adjustment needed to obtain agreement between the two results can then be attributed to departures from unity in the reflectivity of the moon. Specifically we can choose a model in which the dielectric impedance mismatch is the sole source of reflectivity. Thus at normal incidence, we write

$$\left(\frac{\sigma(0)}{A_0}\right)_{\text{moon}} = \left(\frac{\sigma(0)}{A_0}\right)_{\text{metal}} Q^2$$

where Q is the amplitude reflection coefficient. Since the mean scale size of the irregularities is much larger than the impinging wavelength of $\lambda = 3.6$ cm, we may set $Q = (\sqrt{\varepsilon} - 1)/(\sqrt{\varepsilon} + 1)$, where ε is the dielectric constant of the moon's surface. Safran[11] has given for $[\sigma(0)/A_0]_{\text{moon}}$ a value of -1.7 db $\pm$ 1.5 db. The laboratory result is $[\sigma(0)/A_0]_{\text{metal}} = 14.5$ db $\pm$ 0.5 db for surface No. 1. Using these values, we obtain $\varepsilon = 1.9 \pm 0.3$ for the dielectric constant of the moon at microwave frequencies. This value of ε is close to that for certain porous materials such as loosely packed sand[4] and pumice[4,12] (porous volcanic glass).

Since we have discussed the close correspondence of the charcteristics of the rough sea, the moon, and the laboratory-prepared random surfaces, it is well to note that observers have obtained a range of differing empirical results on the wavelength dependence of the backscattering cross section of the sea. All find a relation of the form $\sigma \propto \lambda^{-\gamma}$, but the value of γ ranges from 0 to 4 (Skolink,[13] p. 531). The Naval Research Laboratory[13] data at grazing angles indicates $\gamma \approx 1$. Since (*i*) and (*ii*) of the Conclusions apply, the moon data at $\lambda = 3.6$ cm and 68 cm reproduced in Fig. 17 show also $\gamma \approx 1$ at grazing incidence. This is consistent with our sixth conclusion given above. A recent theoretical study[8] predicts [(7) and (18) of Ref. 8] that the backscattering cross section per unit area *at normal incidence* is proportional to λ^2. Our results do not confirm these predictions.

VIII. ACKNOWLEDGMENT

We are indebted to E. Krauth for assistance in the preparation of the rough aluminum surfaces, to J. A. Giordmaine for providing the MgO slab, to C. Sandahl's group for contour traces of the surfaces, to P. Rosenthal's group at Cornell Aeronautical Laboratories for programming the statistical analysis, and to J. Quackenbush for assistance in setting up the experiment and for taking the scatter data. We also acknowledge the encouragement and support given by N. Levine and wish to thank I. Jacobs, H. G. Cooper and W. E. Danielson for helpful discussions.

REFERENCES

1. Davies, H. and Macfarlane, G. G., Radar Echoes from the Sea Surface at Centimetre Wavelengths, Proc. Phys. Soc., *58*, 1948, pp. 717–729.
2. Grant, C. R. and Yaplee, B. S., Backscattering from Water and Land at Centimeter and Millimeter Wavelengths, Proc. IRE, *45*, July, 1957, pp. 976–983.
3. Wiltse, J. C., Schlesinger, S. P., and Johnson, C. M., Backscattering Characteristics of the Sea in the Region from 10 to 50 kmc, Proc. IRE, *45*, February, 1957, pp. 220–228.
4. Evans, J. V. and Pettengill, G. H., The Scattering Behavior of the Moon at Wavelengths of 3.6, 68, and 784 Centimeters, J. Geophys. Res., *68*, January 15, 1963, pp. 423–447.
5. Corrsin, S. and Kistler, A. L., Free-Stream Boundaries of Turbulent Flows, NACA Report 1244, 1955.
6. Schapker, R. L., Turbulence Front Statistics of Wakes from Bodies in High-Speed Flight, AVCO Everett Research Note 530, 1965.
7. Katz, I., Radar Reflectivity of the Earth's Surface, The Johns Hopkins University, Appl. Phys. Lab. Tech. Digest, January–February, 1963.
8. Beckmann, P., Radar Backscatter from the Moon, J. Geophys. Res., *70*, May 15, 1965, pp. 2345–2349.
9. Lynn, V. L., Sohigan, M. D., and Crocker, E. A., Radar Observations of the Moon at a Wavelength of 8.6 Millimeters, J. Geophys. Res., *69*, 1964, pp. 781–783.

10. Evans, J. V., private communication.
11. Safran, H., Backscattering Properties of Moon and Earth at X-Band, AIAA Journal, January, 1964, pp. 100–101.
12. Brunschwig, M., et al, Estimation of the Physical Constants of the Lunar Surface, The University of Michigan, Report No. 3544-1-F, November, 1960. (Table IV, p. 16 and Figure 6, p. 20.)
13. Skolnik, M. I., *Introduction to Radar Systems*, McGraw-Hill Book Co., Inc., 1962, p. 531.